Antitumor Pentamethylcyclopentadienyl Rhodium Complexes of Maltol and Allomaltol: Synthesis, Solution Speciation and Bioactivity

Orsolya Dömötör[a], Sabine Aicher[b], Melanie Schmidlehner[b], Maria S. Novak[b], Alexander Roller[b], Michael A. Jakupec[b,c], Wolfgang Kandioller[b,c], Christian G. Hartinger[d], Bernhard K. Keppler[b,c], Éva A. Enyedy[a*]

[a] Department of Inorganic and Analytical Chemistry, University of Szeged, Dóm tér 7, H-6720 Szeged, Hungary

[b] Institute of Inorganic Chemistry, University of Vienna, Waehringer Str. 42, A-1090 Vienna, Austria

[c] University of Vienna, Research Platform Translational Cancer Therapy Research, Waehringer Str. 42, A-1090 Vienna, Austria

[d] School of Chemical Sciences, The University of Auckland, PB: 92019, 1142 Auckland, New Zealand

Keywords: Stability Constants; Equilibria; Cytotoxicity; X-ray Crystal Structure; Hydroxypyrones; Rhodium(III)

* Corresponding author: Fax: +36 62 420505
E-mail address: enyedy@chem.u-szeged.hu (E. A. Enyedy)

ABSTRACT

The reaction of the dimer [Rh^{III}(pentamethylcyclopentadienyl)(μ-Cl)Cl]$_2$ ([Rh^{III}(Cp*)(μ-Cl)Cl]$_2$) with the hydroxypyrone ligands maltol and allomaltol affords complexes of the general formula [Rh^{III}(Cp*)(L)Cl] under standard and microwave conditions. The organometallic compounds were characterized by standard analytical methods and in the case of the allomaltol derivative in the solid state by single-crystal X-ray diffraction analysis. The complexes showed similar cytotoxicity profiles and were proved to be moderately active against various human cancer cell lines. The stoichiometry and stability of these complexes were determined in aqueous solution by pH-potentiometry, ^{1}H NMR spectroscopy and UV-visible spectrophotometry. Speciation was studied in the presence and in the absence of chloride ions. Hydrolysis of [Rh^{III}(Cp*)$(H_2O)_3$]$^{2+}$ gave dimeric mixed hydroxido species [(Rh^{III}(Cp*))$_2$(μ-OH)$_3$]$^+$ and [(Rh^{III}(Cp*))$_2$(μ-OH)$_2$Z$_2$] (Z = H_2O/Cl^-). Formation of the mononuclear complexes [Rh^{III}(Cp*)(L)Z] of maltol and allomaltol with similar and moderate stability was found. These species predominate at physiological pH and decompose only partially at micromolar concentrations. In addition, hydrolysis of the aqua complex or the chlorido/hydroxido co-ligand exchange resulted in the formation of the mixed-hydroxido species [Rh^{III}(Cp*)(L)(OH)] in the basic pH range. Replacement of the chlorido by an aqua ligand in the complex [Rh^{III}(Cp*)(L)Cl] was monitored and with the help of the equilibrium constants the extent of aquation at various chloride concentrations of the extra- and intracellular milieu can be predicted. Complexation of these Rh^{III} complexes was compared to analogous [Ru^{II}(η^6-*p*-cymene)] species and higher conditional stabilities were found in the case of the Rh^{III} compounds at pH 7.4.

1. Introduction

In spite of the clinical success of cisplatin, cis-diamminedichloridoplatinum(II), and its derivatives there is an on-going demand for the development of novel types of antitumor agents due to the two main disadvantages of these Pt-containing drugs; namely the low efficacy against widespread tumors, intrinsic and acquired resistance of neoplams and severe side effects accompanying tumors [1-3]. In this context, complexes of the neighboring transition metals such as Ru, Os, Ir and Rh have received considerable attention as possible alternatives to Pt anticancer agents. The most promising metal-based anticancer drug candidates in clinical trials are the Ru^{III}-based *trans*-[tetrachlorido(1H-imidazole)(dimethylsulfoxide-κ*S*)ruthenate(III)] (NAMI-A) being active against metastases [4], indazolium *trans*-[tetrachloridobis(1H-indazole)ruthenate(III)] complexes KP1019 [5] and its sodium analogue KP1339 [6], which are active against a variety of solid tumors. These Ru compounds exhibit low general toxicity, which contrasts to the pharmacological properties of Pt drugs. Organometallic half-sandwich η^6-arene (such as *p*-cymene, biphenyl) or η^5-cyclopentadienyl complexes of Ru and Os are extensively investigated, however relatively few studies are focused on related Rh(II/III) compounds with antitumor activity [7-9]. The anticancer properties of $RhCl_3$ have been known for many decades [10]. Simple complexes such as *mer*-$[RhCl_3(NH_3)_3]$ or *mer,cis*-$[RhCl_3(DMSO)_2(NH_3)]$ were also found to be anticancer active *in vivo* [11,12]. Various dirhodium(II,II) complexes have also been reported by Dunbar *et al.* such as carboxylates which are able to inhibit cell viability of the human cancer cells and DNA was found to be their cellular target via the potentially intercalation forming DNA interstrand cross-links [13,14]. Numerous half-sandwich complexes of Rh such as $[(\eta^5\text{-}C_5Me_5)Rh(LL)Cl]$, where (LL) is a bidentate polypyridyl ligand, were prepared as well and their antiproliferative properties in human cancer cell lines were tested by Sheldrick and co-workers [15-17]. Rh^{III} is isoelectronic with Ru^{II} and Pt^{IV}, air-stable and forms low-spin complexes. $[Rh(H_2O)_6]^{3+}$ features slow ligand exchange processes which may be related to the low interest in Rh^{III} compounds for anticancer drug development [7]. The kinetic inertness can be overcome via the coordination of neutral arene or especially by anionic (pentamethyl)cyclopentadienyl ligands [7]. The nature of the co-ligands in the half-sandwich complexes strongly affects the stability, reactivity and biological activity. On the other hand, metallodrugs are generally considered as prodrugs and thus can undergo transformation processes in the aqueous phase under physiological conditions [18]. Therefore, the knowledge of their speciation and the most plausible chemical species formed in aqueous solution in the

biologically relevant pH range is a mandatory prerequisite for understanding the alterations in their biological activity [19].

Recently, we reported Rh(III)-η^5-pentamethylcyclopentadienyl [Rh^{III}(Cp*)] complexes bearing 3-hydroxyflavone ligands but their anticancer activity could not be tested as a result of the very limited solubility in aqueous solution [20]. Hydroxyflavone compounds can be considered as derivatives of the 3-hydroxy-4-pyrone such as the naturally occurring 3-hydroxy-2-methyl-pyran-4(1H)-one (maltol). *In vitro* biological tests show moderate cytotoxicity of [Ru^{II}(η^6-*p*-cymene)] complexes of hydroxypyrones against cancer cells [21-23], but no data are available for analogous [Rh^{III}(Cp*)] complexes. In the present work, we report the [Rh^{III}(Cp*)(L)Cl] complexes of maltol and 5-hydroxy-2-methyl-pyran-4(1H)-one (allomaltol) (Chart 1) and their biological activity in human cancer cells. Solution equilibria of these metal complexes were studied in detail by the combination of various methods such as pH-potentiometry, UV-visible (UV-Vis) and ^{1}H NMR spectroscopy in order to determine the stoichiometry and stability of complexes formed in aqueous solution. The chlorido/aqua co-ligand exchange reactions in the species [Rh^{III}(Cp*)(L)Cl] of maltol and allomaltol was also monitored, which may affect the biological activity as in case of [Ru^{II}(η^6-*p*-cymene)(L)Cl] complexes [24]. Stability constants of the complexes were determined in the presence and in the absence of chloride ions. Hydrolysis of [Rh^{III}(Cp*)$(H_2O)_3$]$^{2+}$ (Chart 1) was explored under various chloride concentrations.

Chart 1

2. Experimental

2.1. Chemicals

All solvents were of analytical grade and used without further purification. Maltol, sodium methoxide, KCl, KNO_3, $AgNO_3$, HCl, HNO_3 and KOH were purchased from Sigma-Aldrich and used without further purification. Allomaltol [25], dimeric rhodium precursor [Rh^{III}(Cp*)(μ-Cl)Cl]$_2$ and chlorido[2-methyl-3-(oxo-κO)-pyran-4(1H)-onato-κO](η^5-1,2,3,4,5-pentamethylcyclopentadienyl)rhodium(III) (**1a**) were prepared according to literature procedures [26,27]. Microwave-assisted reactions were performed in a CEM Explorer 12 Hybrid apparatus. Melting points were determined with a Büchi Melting Point B-540 apparatus. Elemental analyses were carried out with a Perkin Elmer 2400 CHN Elemental

Analyser by the Microanalytical Laboratory of the University of Vienna. NMR spectra were recorded at 25 °C using a Bruker FT-NMR spectrometer Avance III^{TM} 500 MHz. ^{1}H-NMR spectra were measured at 500.10 MHz and ^{13}C{1H}-NMR spectra at 125.75 MHz in d_4-MeOH. The 2D NMR spectra were measured in a gradient-enhanced mode. The exact concentration of the ligand stock solutions together with the proton dissociation constants were determined the by pH-potentiometric titrations with the help of the computer program HYPERQUAD [28]. A stock solution of $[Rh^{III}(Cp^*)Z_3]$ (where Z = H_2O and/or Cl^-; charges are omitted for simplicity) was obtained by dissolving a known amount of $[Rh^{III}(Cp^*)(\mu\text{-}Cl)Cl]_2$ in water, while the stock solution of $[Rh^{III}(Cp^*)(H_2O)_3](NO_3)_2$ was obtained from an aqueous solution of $[Rh^{III}(Cp^*)(\mu_2\text{-}Cl)Cl]_2$ after removal of chloride ions using equivalent amounts of $AgNO_3$. The exact concentrations of the $[Rh^{III}(Cp^*)]$ stock solutions (with or without chloride) were checked by pH-potentiometric titrations with refinement of the stability constants for $[Rh^{III}_2(Cp^*)_2(\text{hydroxido})_i]$ (i = 2 or 3) complexes.

2.2. pH-Potentiometric measurements

The pH-potentiometric measurements for determination of the proton dissociation constants of the ligands and the overall stability constants of the Rh^{III}-Cp* complexes were carried out at 25.0 ± 0.1 °C in water and at an ionic strength of 0.20 M KCl or KNO_3 used for keeping the activity coefficients constant. The titrations were performed with carbonate-free KOH solution (0.20 M). The exact concentrations of HCl, HNO_3 and KOH solutions were determined by pH-potentiometric titrations. An Orion 710A pH-meter equipped with a Metrohm combined electrode (type 6.0234.100) and a Metrohm 665 Dosimat burette were used for the pH-potentiometric measurements. The electrode system was calibrated to the pH = $-\log[H^+]$ scale by means of blank titrations (strong acid *vs.* strong base: HCl/HNO_3 *vs.* KOH), as suggested by Irving *et al.* [29]. The average water ionization constant, pK_w, was determined as 13.76 ± 0.01 at 25.0 °C, I = 0.20 M (KCl, KNO_3), which corresponds well to the literature [30]. The reproducibility of the titration points included in the calculations was within 0.005 pH units. The pH-potentiometric titrations were performed in the pH range 2.0−11.5. The initial volume of the samples was 10.0 mL. The ligand concentration was 1.0−2.0 mM and metal ion-to-ligand ratios of 1:1 to 1:3 were used. The accepted fitting of the titration curves was always less than 10 μL. Samples were degassed by bubbling purified

argon through them for *ca.* 10 min prior to the measurements and it was also passed over the solutions during the titrations.

The computer program PSEQUAD [31] was utilized to establish the stoichiometry of the complexes and to calculate the overall stability constants. $\beta(M_pL_qH_r)$ is defined for the general equilibrium:

$$pM + qL + rH \rightleftharpoons M_pL_qH_r \text{ as } \beta(M_pL_qH_r) = [M_pL_qH_r]/[M]^p[L]^q[H]^r \quad (1)$$

where M denotes the metal moiety [Rh^{III}(Cp*)] and L the completely deprotonated ligand. Logβ values of the various [Rh^{III}(Cp*)(hydroxido)] complexes were calculated based on the pH-potentiometric titration data in the absence and presence of chloride ions. In all calculations exclusively titration data were used from experiments in which no precipitate was visible in the reaction mixture.

2.3. UV–Vis spectrophotometric and ^{1}H NMR measurements

A Hewlett Packard 8452A diode array spectrophotometer was used to record the UV-Vis spectra in the interval 200–800 nm. The path length was 1 cm. The spectrophotometric titrations were performed with samples containing only the ligands (0.1 mM), [Rh^{III}(Cp*)Z_3] (0.16 mM) or a 1:1 molar ratio of [Rh^{III}(Cp*)Z_3] and ligand (0.22 mM) over the pH range 2.0–11.5 at an ionic strength of 0.20 M (KCl or KNO_3) and at 25.0 ± 0.1 °C. UV-Vis spectra were also recorded to study the H_2O/Cl^- exchange processes in the [Rh^{III}(Cp*)(L)Z] complexes at pH 7.40 (maltol) or 7.05 (allomaltol) in dependence of the Cl^- concentration (0–280 μM). Stability constants for this exchange process were calculated with the computer program PSEQUAD [31].

^{1}H NMR studies were carried out on a Bruker Ultrashield 500 Plus instrument. 4,4-Dimethyl-4-silapentane-1-sulfonic acid was used as an internal NMR standard. The ligands were dissolved in a 10% (v/v) D_2O/H_2O mixture to yield a concentration of 1 or 2 mM and were titrated at 25 °C, at I = 0.20 M (KCl or KNO_3) in absence or presence of [Rh^{III}(Cp*)Z_3] at 1:1 or 1:2 metal-to-ligand ratios.

2.4. Synthesis of [Rh^{III}(Cp)] complexes of maltol and allomaltol*

Chlorido[2-methyl-3-(oxo-κO)-pyran-4(1H)-onato-κO](η^5-1,2,3,4,5-pentamethylcyclopentadienyl)rhodium(III) **1a**

Microwave-assisted synthesis: 3-Hydroxy-2-methyl-pyran-4(1H)-one (23 mg, 0.18 mmol, 1 eq) and sodium methoxide (11 mg, 0.20 mmol, 1.1 eq) were dissolved in dry methanol (4 mL) and stirred for 15 min in a microwave vial. $[Rh^{III}(Cp^*)(\mu\text{-}Cl)Cl]_2$ (50 mg, 0.08 mmol, 0.9 eq) was added in one portion and the reaction vessel was placed in the microwave instrument. The reaction mixture was irradiated for 30 s with a final temperature of 60 °C (max. 10 W). The solvent was removed under reduced pressure, the residue was dissolved in CH_2Cl_2 and the solution was filtered. The volume was reduced to ~2 mL and diethyl ether was added. The mixture was stored overnight at 4 °C and the formed crystals were seperated by filtration and dried *in vacuo* (46 mg, 71%).

Mp: > 178 °C (decomp.); ^{1}H NMR (500.10 MHz, d_4-MeOH): δ = 1.72 (s, 15H, $-CH_{3,Cp^*}$), 2.43 (s, 3H, $-CH_{3,Pyr}$), 6.58 (d, 1H, ^3J(H,H) = 6 Hz, H4), 7.91 (d, 1H, ^3J(H,H) = 6 Hz, H5); ^{13}C NMR (125.75 MHz, d_4-MeOH): δ = 7.4 ($-CH_{3,Cp^*}$), 13.1 ($-CH_{3,Pyr}$), 92.1 (C_{Cp^*}), 113.5 (C5), 153.3 (C6), 154.1 (C2), 156.2 (C3), 182.0 (C4); Elemental analysis calcd. (%) for $C_{16}H_{20}ClO_3Rh \cdot 0.25H_2O$: C 47.14, H 5.19 found C 47.28, H 4.79.

Chlorido[2-methyl-5-(oxo-κO)-pyran-4(1H)-onato-κO](η^5-1,2,3,4,5-pentamethylcyclopentadienyl)rhodium(III) **1b**

Standard procedure: 5-Hydroxy-2-methyl-pyran-4(1H)-one (91 mg, 0.72 mmol, 1 eq) and sodium methoxide (43 mg, 0.79 mmol, 1.1 eq) were dissolved in dry methanol (20 mL) and $[Rh^{III}(Cp^*)(\mu\text{-}Cl)Cl]_2$ (200 mg, 0.32 mmol, 0.9 eq) was added in one portion. The obtained deep red solution was stirred for 18 h at room temperature. The solvent was removed under reduced pressure; the residue was dissolved in CH_2Cl_2, filtered, concentrated and precipitated with diethyl ether. The orange product was separated by filtration and dried *in vacuo* (116 mg, 45%).

Microwave-assisted synthesis: 5-Hydroxy-2-methyl-pyran-4(1H)-one (23 mg, 0.18 mmol, 1 eq) and sodium methoxide (11 mg, 0.20 mmol, 1.1 eq) were dissolved in dry methanol (3-4 mL) and stirred for 15 min in a microwave vial. $[Rh^{III}(Cp^*)(\mu\text{-}Cl)Cl]_2$ (50 mg, 0.08 mmol, 0.9 eq) was added in one portion and the reaction vessel was placed in the microwave instrument. The reaction mixture was irradiated for 30 s (max. 10 W) with a final temperature of 60 °C. The solvent was removed under reduced pressure, the residue dissolved in CH_2Cl_2 and filtered. The volume was reduced to ~2 mL and diethyl ether was added. The mixture was

stored overnight at 4 °C and the formed crystals were collected by filtration and dried *in vacuo* (46 mg, 71%).

Mp: >213 °C (decomp.); ^{1}H NMR (500.10 MHz, d_4-MeOH): δ = 1.72 (s, 15H, -$CH_{3,Cp*}$), 2.34 (s, 3H, -$CH_{3,Pyr}$), 6.46 (s, 1H , H4), 7.75 (s, H5); ^{13}C NMR (125.75 MHz, d_4-MeOH): δ = 7.4 (-$CH_{3,Cp*}$), 18.1 (-CH_{3Pyr}), 92.1 (C_{Cp*}), 109.5 (C5), 141.2 (C6), 157.6 (C2), 166.7 (C3), 184.6 (C4); Elemental analysis calcd. (%) for $C_{16}H_{20}ClO_3Rh \cdot H_2O$: C 46.11, H 5.32 found C 45.90, H 4.91.

2.5. Crystallographic structure determination

For X-ray diffraction analysis single crystals of **1b** were obtained by using the slow diffusion method from CH_2Cl_2/diethyl ether. The single crystals were analyzed on a Bruker D8 Venture diffractometer at 100 K. The single crystal was positioned at 45 mm from the detector and 1363 frames for 16 s exposure time over 0.4° scan width were measured. The data were processed using the SAINT software package [32]. The structures were solved by direct methods and refined by full-matrix least-squares techniques. Non-hydrogen atoms were refined with anisotropic displacement parameters. Hydrogen atoms were inserted at calculated positions and refined with a riding model. The following computer programs were used: structure solution, SHELXS-97 [33]; refinement, SHELXL-2013 [33]; OLEX2 [34]; SHELXLE [35]; molecular diagrams, ORTEP-3 [36]; scattering factors [37]. The crystallographic data files for **1b** have been deposited with the Cambridge Crystallographic Database as CCDC 966490.

2.6. Cell lines and culture conditions, cytotoxicity tests in cancer cell lines

Cell lines and culture conditions: CH1 cells originate from an ascites sample of a patient with an adenocarcinoma of the ovary and were a gift from Lloyd R. Kelland, CRC Centre for Cancer Therapeutics, Institute of Cancer Research, Sutton, UK. SW480 (human adenocarcinoma of the colon) and A549 (human non-small cell lung cancer) cells were provided by Brigitte Marian (Institute of Cancer Research, Department of Medicine I, Medical University of Vienna, Austria). All cell culture reagents were obtained from Sigma-Aldrich Austria and plastic ware from Starlab Germany. Cells were grown in 75 cm² culture flasks (Iwaki) as adherent monolayer cultures in Minimum Essential Medium (MEM)

supplemented with 10% heat inactivated fetal calf serum, 1 mM sodium pyruvate, 4 mM L-glutamine and 1% non-essential amino acids (from 100x ready-to-use stock). Cultures were maintained at 37 °C in humidified atmosphere containing 95% air and 5% CO_2.

MTT assay: Cytotoxicity was determined by the colorimetric MTT [3-(4,5-dimethyl-2-thiazolyl)-2,5-diphenyl-2H-tetrazolium bromide] microculture assay. For this purpose, cells were harvested from culture flasks by trypsinisation and seeded in 100 µL/well aliquots into 96-well microculture plates. Cell densities of 1.0×10^3 cells/well (CH1), 2.0×10^3 cells/well (SW480) and 3.0×10^3 cells/well (A549) were chosen in order to ensure exponential growth of untreated controls throughout the experiment. Cells were allowed to settle and resume exponential growth in drug-free complete culture medium for 24 h. Stock solutions of the test compounds in DMSO were diluted in complete culture medium and added to the plates (100 µL/well) where the maximum DMSO content did not exceed 0.5%. After 96 h of exposure, all media were replaced with 100 µL/well of MTT/RPMI1640 mixture (six parts of RPMI1640 medium supplemented with 10% heat-inactivated fetal bovine serum and 4 mM L-glutamine; one part of 5 mg/mL MTT reagent in phosphate-buffered saline). After incubation for 4 h, the supernatants were removed, and the formazan crystals formed by viable cells were dissolved in 150 µL DMSO per well. Optical densities at 550 nm were measured with a microplate reader (BioTek ELx808), by using a reference wavelength of 690 nm to correct for unspecific absorption. The quantity of viable cells was expressed in terms of T/C values by comparison to untreated controls, and 50% inhibitory concentrations (IC_{50}) were calculated from concentration-effect curves by interpolation. Evaluation is based on means from three independent experiments, each comprising three replicates per concentration level.

3. Results and discussion

3.1. Synthesis of organometallic Rh(III) complexes and characterization

The Rh^{III} precursor $[Rh^{III}(Cp^*)(\mu\text{-}Cl)Cl]_2$ was synthesized according to literature procedures by reaction of $RhCl_3$ with pentamethylcyclopentadiene (Cp*) [26]. The maltol-based Rh^{III} complex was obtained according to the procedure described by Abbott *et al.* [27], which was adapted to prepare the analogous allomaltol organometallic complex. The ligand was deprotonated by sodium methoxide, followed by conversion with the Rh^{III} dimer at room temperature (Scheme 1). The isolated yield was found to be slightly lower (71%) compared to

the maltol complex (90%). Recently, Severin and coworkers reported the microwave-assisted synthesis of dimeric $[Ru^{II}(\eta^6\text{-}p\text{-cymene})(\mu\text{-Cl})Cl]_2$ and $[Rh^{III}(Cp^*)(\mu\text{-Cl})Cl]_2$ [38] at 140 °C which decreased the reaction time from several hours at reflux to minutes. We decided to investigate the potential of this powerful tool for the synthesis of organorhodium compounds **1a** and **1b**. Several reactions were performed to determine the optimal microwave conditions for the coordination reaction. It was found that 60 °C was the optimal temperature for the coordination to avoid decomposition processes at higher temperatures or undesired side reactions at longer reaction times. The full conversion of the educts was observed after 30 seconds of irradiation and the complexes were isolated in good yields after work up.

Scheme 1

The organometallic Rh^{III} complexes were characterized by means of standard analytical methods and their purity was confirmed by elemental analysis. The ^1H NMR spectra supported the coordination of the organorhodium fragment. The α-proton next to the carbonyl group of the pyrone ring was shifted to higher fields upon coordination of the metal ion, whereas the signal assigned to the β-proton next to the ether functionality of the backbone was found slightly low-field shifted compared to the free ligands (Figs. S1 and S2), which is comparable to the analogues Ru^{II} complexes [39].

Single crystals of **1b** were obtained by the slow diffusion method from CH_2Cl_2/diethylether and the result of the X-ray diffraction study is shown in Fig. 1. Crystal data, data collection parameters, and structure refinement details are given in Table 1. In this complex the Rh^{III} exhibits a pseudo-octahedral geometry and the Cp* moiety occupies three coordination sites, while the allomaltolato ligand binds in a bidentate manner via its (O,O) donor atoms and the coordination sphere is completed with a chlorido ligand. The coordination sphere leads to a chiral center at the rhodium atom and both enantiomers were found in the unit cell. In general, the Rh^{III}–ligand bond lengths and angles were found in the same range as for $[Rh^{III}(Cp^*)(maltolato)Cl]$ **1a** [27].

Fig. 1

Table 1

3.2. Hydrolytic processes of $[Rh^{III}(Cp^*)Z_3]$ in absence and presence of chloride ions

The hydrolysis of the half-sandwich complex $[Rh^{III}(Cp^*)Z_3]$ ($Z = H_2O$ or Cl^-) was studied by pH-potentiometric and ^1H NMR titrations at ionic strengths such as 0.2 M KNO_3, 0.2 and 0.1 M KCl, and it was found that the equilibria could be reached quite fast in the whole studied

pH range (always less than ~6 min). The stoichiometries and overall stability constants of the formed dinuclear hydrolysis products were determined based on the findings of both methods (Table 2).

Table 2

According to literature data [$Rh^{III}(Cp^*)$] appears as $[Rh^{III}(Cp^*)(H_2O)_3]^{2+}$ in the absence of chloride at acidic pH values following the dissolution of the dimer $[Rh^{III}(Cp^*)(\mu\text{-}Cl)Cl]_2$. This aqua complex has a pseudooctahedral piano-stool type geometry proved by X-ray crystallography [40]. The aqua ligands in $[Rh^{III}(Cp^*)(H_2O)_3]^{2+}$ are in the presence of chlorides most probably partially or completely substituted by chloride ions, which is reflected in the lowered chemical shifts of the methyl groups of the Cp* moiety measured at acidic pH values (Fig. 2, Table S1).

Fig. 2

While the intensity of the peak assigned to the Cp* protons of $[Rh^{III}(Cp^*)(Z)_3]$ (Z = H_2O or Cl^-) decreases, a new peak appears at lower chemical shifts above pH ~5.3 and ~7 in the absence and presence of Cl^-, respectively (Fig. 2). This peak migrates further to lower chemical shifts with increasing pH values up to pH ~8 (with KNO_3) or ~9 (with KCl) and thereafter it remains unchanged These findings strongly support the formation of a hydroxido species in the intermediate pH range. This is a fast exchange process with respect to the NMR time scale with the hydroxido complex predominating in the basic pH range. This latter species is most probably the tris(μ-hydroxido) dinuclear complex $[(Rh^{III}(Cp^*))_2(\mu\text{-}OH)_3]^+$ (annotated $[M_2H_{-3}]$) which forms in both media as its chemical shift is identical independent of the presence of nitrate or chloride counter ions (Fig. 2, Table S1). The structure of $[M_2H_{-3}]$ was determined by X-ray crystallography [41] and its formation was also shown previously by Eisen *et al.* at high pH in the absence of Cl^- [40]. The pH-potentiometric titration curves of $[Rh^{III}(Cp^*)Z_3]$ recorded in 0.2 M KNO_3, 0.1 or 0.2 M KCl media reveal that the hydrolysis starts at higher pH in the presence of chloride ions and inflection points are seen at pH *ca.* 5.9, 7.0 and 7.3, respectively (Figs. 3 and S3). Titration curves also show the consumption of 1.5 base equivalents per $[Rh^{III}(Cp^*)Z_3]$ indicating that $[M_2H_{-3}]$ is the major species above pH ~8 (with KNO_3) and ~9 (with 0.2. M KCl). However, the calculated titrations curves could be fitted slightly better to the measured ones in all cases by including $[(Rh^{III}(Cp^*))_2(\mu\text{-}OH)_2Z_2]$ (*i.e.* $[M_2H_{-2}]$) as a minor component in the speciation models (Figs. 3 and S3, Table 2). Formation of an intermediate complex $[(Rh^{III}(Cp^*))_2(\mu\text{-}OH)_2(H_2O)_2]^{2+}$ was also assumed by

Eisen *et al.*, however the overlapping hydrolytic processes could not be deconvoluted and no stability data were provided [40].

Fig. 3

Table 2

Concentration distribution curves were calculated on the basis of the stability constants of the hydroxido complexes obtained by pH-potentiometry (see Fig. 2). The ^{1}H NMR signals of the monomeric and dinuclear species were separated well enough in the case of the nitrate-containing solutions to integrate them and molar fractions of the metal ion could be calculated (Fig. 2a), which are in a good agreement with the pH-potentiometry data. The stability data (Table 2) and the concentration distribution curves clearly reveal that chloride ions suppress the hydrolysis and shift hydrolysis processes to the higher pH range. It is noteworthy that the same trend was shown for the isoelectric species $[Ru^{II}(\eta^6\text{-}p\text{-cymene})Z_3]^{2+}$ [42], although the tendency of $[Rh^{III}(Cp^*)Z_3]$ to hydrolyze is undoubtedly weaker.

3.3. Solution equilibria of $[Rh^{III}(Cp^*)Z_3]$ complexes of maltol and allomaltol in chloride-free and chloride-containing media

The proton dissociation constants of the studied ligands maltol and allomaltol were determined by pH-potentiometry and are in reasonably good agreement with those reported in literature (Table 3) [43,44]. The proton dissociation constants of these hydroxypyrone ligands can be attributed to the deprotonation of the hydroxyl functional group and allomaltol has the lower pK_a value.

Table 3

The complex formation processes of $[Rh^{III}(Cp^*)(Z)_3]$ with maltol and allomaltol were investigated by the combined use of pH-potentiometric, ^{1}H NMR and UV-Vis titrations in the absence and presence of 0.2 M chloride in pure aqueous solutions due to the excellent solubility of the complexes (up to 10 mM). The complex formation equilibrium establishes quickly in both media and quite similar speciation was found in all cases. The stoichiometries of the metal complexes and their overall stability constants furnishing the best fits to the experimental data are listed in Table 3. Formation of only mono-ligand complexes such as [ML] (as $[Rh^{III}(Cp^*)(L)Z]$) and [MLH$_{-1}$] (as $[Rh^{III}(Cp^*)(L)H_{-1}]$) was detected when studying maltol independent of the conditions but was not observed in the case of allomaltol. Representative concentration distribution curves are shown in Fig. 4 for the $[Rh^{III}(Cp^*)(Z)_3]$–allomaltol system in chloride-free medium. It is noteworthy that the hydrolysis product

[MLH_{-1}] of the allomaltol complex could not be detected in the chloride-containing solution. Due to the possible coordination of the chloride ions in the species [$Rh^{III}(Cp^*)Z_3$], [$(Rh^{III}(Cp^*))_2(\mu\text{-}OH)_2Z_2$] and [$Rh^{III}(Cp^*)(L)Z$] by replacing partly the aqua ligands, the stability data for the 0.2 M KCl-containing medium are regarded as conditional stability constants and are valid only under the given conditions.

Fig. 4

According to the pH-potentiometric titration curves the complex formation with maltol starts already at pH ~2 in the nitrate-containing system, while only at pH > 4 in the presence of chloride. This is in good agreement with the pH-dependent ^1H NMR data (see representative spectra for maltol in Fig. 5 in the presence of chloride ions).

Fig. 5

A similar trend was seen in the case of allomaltol (Figs. S4, S5). Since slow ligand-exchange processes were observed in the ^1H NMR spectra of the [$Rh^{III}(Cp^*)(Z)_3$]–ligand systems with respect to the NMR time scale ($t_{1/2}$(obs) > ~1 ms), peaks belonging to the protons of the free or bound ligand and to the bound or non-bound Cp* moiety could be detected separately. The formation of species [MLZ] of maltol can be observed at pH > 4 (Fig. 5). Two parallel processes can be detected in the basic pH range, namely the upfield shift of the peak belonging to [MLZ], which indicates the formation of the hydrolysis product [MLH_{-1}], and the appearance of signals assigned to free ligand and the non-bound metal moiety due decomposition of [MLZ]. The integrated peak areas were converted to molar fractions, which were also determined on the basis of the stability constants obtained by pH-potentiometry. Fairly good correlations between the data of both methods were observed in the whole pH range studied. This is shown exemplary for the [$Rh^{III}(Cp^*)(H_2O)_3$]–maltol system in chloride-free medium in Fig. 6. In addition, UV-Vis spectra were also collected for the same system in the pH range 2–11.5 and the detected spectral changes of the charge transfer bands (Fig. 6) strongly correlate to the formation of the [ML] and [MLH_{-1}] species.

Fig. 6

In the species [$Rh^{III}(Cp^*)(L)Z$] the maltol and allomaltol coordinate via the bidentate (O,O)-donor set as it was shown for [$Rh^{III}(Cp^*)$(maltolato)Cl] [27] and [$Rh^{III}(Cp^*)$(allomaltolato)Cl] (Fig. 1) by X-ray crystallography. On the other hand the species of the general formula [$Rh^{III}(Cp^*)(L)H_{-1}$] are considered as mixed hydroxido [$Rh^{III}(Cp^*)(L)(OH)$] species formed by deprotonation of the coordinated water molecule or (partly) by the replacement of the chlorido ligand in chloride-containing medium.

Based on the overall stability constants (Table 3) of the studied [Rh^{III}(Cp*)] complexes it can be concluded that the stability of the corresponding species of maltol and allomaltol is comparable. The different basicities of the ligands can be taken into consideration (log *K**, Table 3) according to the following competition reaction for a more adequate comparison of the stabilities:

$[Rh^{III}(Cp^*)Z_3] + HL \rightleftharpoons [Rh^{III}(Cp^*)(L)Z] + H^+ + 2\ Z$ (Z = H_2O or Cl^-)

Log *K** values demonstrate the similar chelate stability of the complexes of these hydroxypyrone ligands. It is noteworthy that chloride ions as competitive ligands can suppress the formation of the (O,O)-complexes. This is reflected in the higher pH values where the complexation starts (*vide supra*) in the KCl- over the KNO_3-containing medium and in the lower log *K** values.

It should also be noted that the predominant formation of the species [ML*Z*] is found in all cases at physiological pH. The molar fraction of this species depends on its total concentration as it is shown for the [Rh^{III}(Cp*)(Z_3]–allomaltol system in Fig. 7. Partial decomposition can be predicted in the low-micromolar concentration range.

Fig. 7

In the species [Rh^{III}(Cp*)(L)*Z*] the third coordination site is most probably occupied by a water molecule in the absence of chloride. It can be partially (or completely) displaced by a chloride ligand in the KCl-containing milieu or the chlorido complex can undergo hydrolysis after dissolution. The coordination of the labile chloride results in characteristic spectral changes in the UV-Vis spectra of the complexes (Fig. S6), therefore the stepwise stability constants (log *K*'(H_2O/Cl^-) in Table 3) could be estimated for the $[Rh^{III}(Cp^*)L(H_2O)]^+ + Cl^- \rightleftharpoons [Rh^{III}(Cp^*)(L)Cl)] + H_2O$ equilibrium at about neutral pH values where [Rh^{III}(Cp*)(L)*Z*] complexes predominate. Based on the equilibrium constant for the maltol complex concentration distribution curves were calculated for [ML*Z*] species at various chloride concentrations (Fig. 8). According to the H_2O/Cl^- exchange constants, about 76 and 61% of the maltolato and 82 and 71% of the allomaltolato complexes are chlorinated at neutral pH and 0.2 and 0.1 M chloride concentrations, respectively.

Fig. 8

Stability constants of the analogous complexes formed in the [Ru^{II}(η^6-*p*-cymene)]–maltol/allomaltol systems with the stoichiometries [ML] and [MLH_{-1}] are also available in the literature [45,46]. The direct comparison of the overall stability constants of the complexes of [Ru^{II}(η^6-*p*-cymene)] to those of [Rh^{III}(Cp*)] species shows higher values for [Ru^{II}(η^6-*p*-cymene)] complexes, although the tendency of these metal ions to hydrolyze is significantly

different. Thus this fact has to be taken into consideration when the stabilities are considered. To indicate the difference in the metal binding ability of maltol towards [$Ru^{II}(\eta^6$-*p*-cymene)] and [Rh^{III}(Cp*)], pM values were computed at various pH values under the same conditions (Fig. 9). pM values give the negative logarithm of the equilibrium concentrations of the non-bound metal ion ([M], [M_2H_{-2}], [M_2H_{-3}]) under the given conditions. Higher pM values indicate stronger chelating ability.

Fig. 9

The coordination of the ligands to [$Ru^{II}(\eta^6$-*p*-cymene)] starts at more acidic pH values (reflected in the higher log β values of [MLZ] [45,46]) compared with [Rh^{III}(Cp*)]. However, the coordination of maltol to [Rh^{III}(Cp*)] becomes more favorable at pH > ~7 owing to the less pronounced hydrolysis of this metal ion. It can be also noted that maltol is not able to prevent the dissociation of these complexes at pH > ~10.5.

3.4. Cytotoxicity of [Rh^{III}(Cp)] complexes of maltol and allomaltol*

Recently, maltol-derived organometallic complexes were investigated for their anticancer potential, however, only moderate cytotoxicity was observed [39,47]. These observations were explained by the low stability of the compounds under physiological conditions in the presence of biological nucleophiles. Within this work we have shown that coordination of hydroxypyrone ligands to [Rh^{III}(Cp*)] leads to complexes with increased stability at neutral pH. Therefore, the impact of the organorhodium fragment on cytotoxicity was investigated by means of the colorimetric MTT assay in the human cancer cell lines CH1 (ovarian carcinoma), SW480 (colon carcinoma) and A549 (non-small cell lung carcinoma) and compared to the related [$Ru^{II}(\eta^6$-*p*-cymene)] complexes.

Table 4

In general, CH1 cells were found to be the most sensitive of the investigated cell lines and a moderate cytotoxicity was observed for complexes **1a** and **1b** with IC_{50} values of roughly 100 μM, whereas cell lines SW480 were less and A549 least affected by the compounds, corresponding to their more generally lower chemosensitivity. No significant influence of the methyl group position on the pyrone ring was observed, in accordance with the virtually identical stabilities of the complexes. Furthermore, the cytotoxic potency of **1a** was found in the same range as that of the analogous [$Ru^{II}(\eta^6$-*p*-cymene)] complexes [21], but **1b** was

found to be about twice as potent than its Ru^{II} counterpart in all three cell lines, based on comparison of IC_{50} values.

4. Conclusions

The syntheses of [Rh^{III}(Cp*)] complexes of maltol and allomaltol either under standard and microwave conditions are presented. The complexes were obtained by the reaction of the deprotonated 3-hydroxy-4-pyrones with the rhodium precursor [Rh^{III}(Cp*)(μ-Cl)Cl]$_2$ and it was possible to reduce the reaction time from several hours to about 30 seconds under microwave conditions. The cytotoxicity of the complexes was studied in the human cancer cell lines (CH1, SW480 and A549). They were found to exhibit moderate to low cytotoxicity with IC_{50} values of 80–320 μM. As these complexes are well water soluble (up to 10 mM), the solution speciation of [Rh^{III}(Cp*)] complexes of maltol and allomaltol could be characterized in aqueous solution via a combined approach using pH-potentiometry, ^{1}H NMR spectroscopy and UV-Vis spectrophotometry in the absence and presence of chloride ions. The hydrolytic behavior of the species [Rh^{III}(Cp*)$(H_2O)_3$]$^{2+}$ was also studied and formation constants for the dimer hydroxido complexes [(Rh^{III}(Cp*))$_2$(μ-OH)$_3$]$^+$ and [(Rh^{III}(Cp*))$_2$(μ-OH)$_2$Z$_2$] (Z = H_2O/Cl^-) were determined at various chloride concentrations. Exclusive formation of the mono-ligand complexes [ML] and [ML(OH)] with moderate stability were detected. No significant difference between the complex stabilities of the two hydroxypyrones was observed. Chloride ions act as competitive ligands and are able to suppress the formation of [Rh^{III}(Cp*)] complexes to some extent. Notably, species of the type [MLZ] were observed to be predominant at physiological pH, and only partial decomposition of the complexes is expected on the basis of the determined stability constants in the low-micromolar concentration range. Formation of the mixed hydroxido complex [ML(OH)] could be characterized by determination of relatively high pK_a values (9.41–10.60). The aquation of [Rh^{III}(Cp*)(L)Cl] complexes may have impact on the biological activity as Cl^-/H_2O exchange can take place under physiological conditions to different extent depending on the chloride concentrations. Thus, this co-ligand exchange equilibrium was also studied by UV-Vis spectrophotometry. Based on the constants it can be predicted that, *e.g.* ~61% of the maltolato complex exists as the chloride complex at 0.1 M chloride concentration in human blood, and the level of aquation should increase in the cytosol or in the nucleus due to their diminished chloride concentrations. This has important impact on the speciation in biological systems.

The *in vivo* biological activity of an anticancer drug candidate is strongly influenced by pharmacokinetic and pharmacodynamic parameters; therefore the interactions with blood serum proteins such as albumin or with feasible final targets such as DNA or *e.g.* thiolato side chain containing proteins are essential binding events and are currently investigated in our laboratories.

5. Abbreviations

1a	chlorido[2-methyl-3-(oxo-κO)-pyran-4(1H)-onato-κO](η^5-1,2,3,4,5-pentamethylcyclopentadienyl)rhodium(III)
1b	chlorido[2-methyl-5-(oxo-κO)-pyran-4(1H)-onato-κO](η^5-1,2,3,4,5-pentamethylcyclopentadienyl)rhodium(III)
allomaltol	5-hydroxy-2-methyl-pyran-4(1H)-one
maltol	3-hydroxy-2-methyl-pyran-4(1H)-one
Cp*	pentamethylcyclopentadiene
MEM	minimum essential medium
MTT	3-(4,5-dimethyl-2-thiazolyl)-2,5-diphenyl-2H-tetrazolium bromide
$[Rh^{III}(Cp^*)]$	rhodium(III)-η^5-pentamethylcyclopentadienyl
UV-Vis	UV-visible

Acknowledgments

This work was supported by the Hungarian Research Foundation OTKA project PD103905, the Johanna Mahlke née Obermann Foundation and COST Action CM11095. This research was realized in the frames of TÁMOP 4.2.4. A/2-11-1-2012-0001 „National Excellence Program – Elaborating and operating an inland student and researcher personal support system". We thank Ms. Gabriella Kiss for conducting some measurements.

Appendix. Supplementary data

Supplementary data related to this article can be found online at…

References

[1] Y. Jung, S.J. Lippard, Chem. Rev. 107 (2007) 1387–1407.

[2] G.N. Kaluderovic, R. Paschke, Curr. Med. Chem. 18 (2011) 4738–4752.

[3] M.A. Jakupec, M. Galanski, V.B. Arion, C.G. Hartinger, B.K. Keppler, Dalton Trans. (2008) 183–194.

[4] E. Alessio, G. Mestroni, A. Bergamo, G. Sava, Curr. Top. Med. Chem. 4 (2004) 1525–1535.

[5] C.G. Hartinger, M.A. Jakupec, S. Zorbas-Seifried, M. Groessl, A. Egger, W. Berger, H. Zorbas, P.J. Dyson, B.K. Keppler, Chem. Biodiversity 5 (2008) 2140–2155.

[6] P. Heffeter, K. Böck, B. Atil, M.A.R. Hoda, W. Körner, C. Bartel, U. Jungwirth, B.K. Keppler, M. Micksche, W. Berger, G. Koellensperger, J. Biol. Inorg. Chem. 15 (2010) 737–748.

[7] Y. Geldmacher, M. Oleszak, W.S. Sheldrick, Inorg. Chim. Acta 393 (2012) 84–102.

[8] N. Katsaros, A. Anagnostopoulou, Crit. Rev. Oncol. Hemat. 42 (2002) 297–308.

[9] C.H. Leung, H.J. Zhong, D.S.H. Chan, D.L. Ma, Coord. Chem. Rev. 257 (2013) 1764–1776.

[10] A. Taylor, N. Carmichael, Cancer Studies 2 (1953) 36–79.

[11] M.J. Cleare, P.C. Hydes, Met. Ions Biol. Syst. 11 (1980) 1–62.

[12] G. Mestroni, E. Alessio, A. Sessanti o Santi, S. Geremia, A. Bergamo, G. Sava, A. Boccarelli, A. Schettino, M. Coluccia, Inorg. Chim. Acta 273 (1998) 62–71.

[13] S.U. Dunham, H.T. Chifotides, S. Mikulski, A.E. Burr, K.R. Dunbar, Biochemistry 44 (2005) 996–1003.

[14] J.D. Aguirre, A.M. Angeles-Boza, A. Chouai, J.-P. Pellois, C. Turro, K.R. Dunbar, J. Am. Chem. Soc. 131 (2009) 11353–11360.

[15] S. Schäfer, I. Ott, R. Gust, W.S. Sheldrick, Eur. J. Inorg. Chem. 19 (2007) 3034–3046.

[16] M.A. Nazif, R. Rubbiani, H. Alborzinia, I. Kitanovic, S. Wolfl, I. Ott, W.S. Sheldrick, Dalton Trans. 41(2012) 5587–5598.

[17] Y. Geldmacher, K. Splith, I. Kitanovic, H. Alborzinia, S. Can, R. Rubbiani, M.A. Nazif, P. Wefelmeier, A. Prokop, I. Ott, S. Wölfl, I. Neundorf, W.S. Sheldrick, J. Biol. Inorg. Chem. 17 (2012) 631–646

[18] C.G. Hartinger, N. Metzler-Nolte, P.J. Dyson, Organometallics 31 (2012) 5677−5685.

[19] T. Kiss, T. Jakusch, B. Gyurcsik, A. Lakatos, É.A. Enyedy, É. Sija, Coord. Chem. Rev. 256 (2012) 125–132.

[20] M.B. Schwarz, A. Kurzwernhart, A. Roller, W. Kandioller, B.K. Keppler, C.G. Hartinger, ZAAC, 639 (2013) 1648–1654.

[21] W. Kandioller, A. Kurzwernhart, M. Hanif, S.M. Meier, H. Henke, B.K. Keppler, C.G. Hartinger, J. Organomet. Chem. 696 (2011) 999−1010.

[22] R. Fernandez, M. Melchart, A. Habtemariam, S. Parsons, P.J. Sadler, Chem. Eur. J. 10 (2004) 5173–5179.

[23] W. Kandioller, C.G. Hartinger, A.A. Nazarov, J. Kasser, R. John, M.A. Jakupec, V.B. Arion, P.J. Dyson, B.K. Keppler, J. Organomet. Chem. 694 (2009) 922–929.

[24] M. Melchart, A. Habtemariam, O. Novakova, S.A. Moggach, F.P.A. Fabbiani, S. Parsons, V. Brabec, P.J. Sadler, Inorg. Chem. 46 (2007) 8950–8962.

[25] Z.D. Liu, H.H. Khodr, D.Y. Liu, S.L. Lu, R.C. Hider, J. Med. Chem. 42 (1999) 4814–4823.

[26] L. Booth, R.N. Haszeldine, M. Hill. J. Chem. Soc. A (1969) 1299–1303.

[27] A.P. Abbott, G. Capper, D.L . Davies, J. Fawcett, D.R.J. Russell, Chem. Soc. Dalton Trans. (1995) 3709−3713.

[28] P. Gans, A. Sabatini, A. Vacca, Talanta 43 (1996) 1739–1753.

[29] H.M. Irving, M.G. Miles, L.D. Pettit, Anal. Chim. Acta 38 (1967) 475–488.

[30] SCQuery, The IUPAC Stability Constants Database, Academic Software (Version 5.5), Royal Society of Chemistry, 1993–2005.

[31] L. Zékány, I. Nagypál, in: Computational Methods for the Determination of Stability Constants (Ed.: D. L. Leggett), Plenum Press, New York, 1985, pp. 291–353.

[32] M.R. Pressprich, J. Chambers, SAINT + Integration Engine, Program for Crystal Structure Integration, Bruker Analytical X-ray systems: Madison, 2004

[33] G.M. Sheldrick, Acta Cryst. A64 (2008) 112–122.

[34] O.V. Dolomanov, L.J. Bourhis, R.J. Gildea, J.A.K. Howard, H. Puschmann, J. Appl. Cryst. 42 (2009) 339–341.

[35] C.B. Hübschle, B. Dittrich, G.M. Sheldrick, Acta Cryst. A68 (2012) 152.

[36] L.J. Farrugia, J. Appl. Cryst. 30 (1997) 565.

[37] International Tables for X-ray Crystallography. Kluwer Academic Press: Dordrecht, The Netherlands, 1992; Vol. C.

[38] J. Tönnemann, J. Risse, Z. Grote, R. Scopelliti, K. Severin, Eur. J. Inorg. Chem. (2013) 4558–4562.

[39] W. Kandioller, C.G. Hartinger, A.A. Nazarov, M.L. Kuznetsov, R.O. John, C. Bartel, M.A. Jakupec, V.B. Arion, B.K. Keppler, Organometallics 28 (2009) 4249–4251.

[40] M.S. Eisen, A. Haskel, H. Chen, M.M. Olmstead, D.P. Smith, M.F. Maestre, R.H. Fish, Organometallics 14 (1995) 2806−2812.

[41] A. Nutton, P.M. Baily, P.M. Maitlis, J. Chem. Soc. Dalton Trans. (1981) 1997−2002.

[42] L. Bíró, E. Farkas, P. Buglyó, Dalton Trans. 41 (2012) 285–291.

[43] É.A. Enyedy, A. Lakatos, L. Horváth, T. Kiss, J. Inorg. Biochem. 102 (2008) 1473–1485.

[44] É.A. Enyedy, O. Dömötör, E. Varga, T. Kiss, R. Trondl, C.G. Hartinger, B.K. Keppler, J. Inorg. Biochem. 117 (2012) 189−197.

[45] L. Bíró, E. Farkas, P. Buglyó, Dalton Trans. 39 (2010) 10272−10278.

[46] E.A. Enyedy, E. Sija, T. Jakusch, C.G. Hartinger, W. Kandioller, B.K. Keppler, T. Kiss, J. Inorg. Biochem. 127 (2013) 161−168.

[47] A.F.A. Peacock, P.J. Sadler, Chem. Asian J. 3 (2008) 1890−1899.

Legends to Figures/Charts

Chart 1 Chemical structures of maltol (a), allomaltol (b) and $[Rh^{III}(Cp^*)(H_2O)_3]^{2+}$ (c).

Scheme 1 Synthesis of the organometallic Rh^{III} complexes by A) standard procedure (18 h at room temperature) and B) microwave assisted preparation (30 s, < 10 W, 60 °C).

Fig. 1 ORTEP view of $[Rh^{III}(Cp^*)$(allomaltolato)Cl] **1b** at 50% probability level.

Fig. 2 pH-Dependent ^1H NMR spectra and concentration distribution curves of $[Rh^{III}(Cp^*)Z_3]$ (Z = H_2O or Cl^-; M = $Rh^{III}(Cp^*)$) in chloride-free (a) and chloride-containing (b) solutions (left side). Concentration distribution curves for $[MZ_3]$ (grey line), its hydroxido complexes (black lines) and summarized fractions for the hydroxido complexes (dashed line) calculated by the use of their overall stability constants. Molar fractions based on the ^1H NMR peak integrals: $[M(H_2O)_3]$ (●) and $[M_2H_{-i}]$ (○, i = 2 or 3) (right side). {c_M = *1 mM; T = 25 ˚C; I = 0.20 M (KNO₃ or KCl); 10% D_2O*}.

Fig. 3 Representative pH-potentiometric titration curve of $[Rh^{III}(Cp^*)(H_2O)_3]$ in chloride-free aqueous solution (×) and calculated curves confirming (grey solid line) or disproving (grey dotted line) the existence of $[M_2H_{-2}]$ hydroxido species besides $[M_2H_{-3}]$. {c_M = *1.2 mM; T = 25 ˚C; I = 0.20 M (KNO_3)*}.

Fig. 4 Concentration distribution curves of the $[Rh^{III}(Cp^*)(H_2O)_3]$–allomaltol system in chloride-free aqueous solution. {$c_M = c_L$ = *1 mM; T = 25 ˚C; I = 0.20 M (KNO_3)*}.

Fig. 5 Low (a) and high (b) field regions of ^1H NMR spectra of the $[Rh^{III}(Cp^*)Z_3]$–maltol system in chloride-containing aqueous solution recorded at various pH values. The CH(5) (maltol) (a) and CH_3 (Cp*) (b) proton peaks are highlighted. {$c_M = c_L$ = *1 mM; T = 25 ˚C; I = 0.20 M (KCl); 10% D_2O; i = 2 or 3; Z = H_2O or Cl^-*}.

Fig. 6 Concentration distribution curves of the $[Rh^{III}(Cp^*)(H_2O)_3]$–maltol system in chloride-free aqueous solution calculated on the basis of the overall stability constants and ^1H NMR peak integrals: bound (●) and free (○) ligand together with the pH-dependence of the absorbance values at 430 nm for the same system (×). {c_{maltol} = *1 mM* (^1H NMR, *10% D_2O*) and *220 μM* (UV-Vis)*; M : L* = 1:1*; l = 1 cm; T = 25.0 ˚C, I = 0.20 M (KNO_3) }*.

Fig. 7 Concentration distribution curves of the [Rh^{III}(Cp*)Z_3]–allomaltol (1:1) system in chloride-free (grey lines) and chloride-containing (black lines) aqueous solutions as a function of the analytical (total) complex concentrations at pH 7.40. {*T = 25 ˚C; I = 0.20 M (KCl or KNO_3); Z = H_2O or Cl^-*}.

Fig. 8 Chloride-dependent absorbance values at 430 nm (o) and calculated concentration distribution curves for the water/chloride exchange process of the [Rh^{III}(Cp*)$(H_2O)_3$]–maltol system at physiological pH. {$c_M = c_L$ = *0.50 mM; T = 25 ˚C; pH = 7.40)*}.

Fig. 9 pH-dependence of pM values calculated for the [Rh^{III}(Cp*)Z_3]–maltol (solid line) and [Ru^{II}(η^6-*p*-cymene)Z_3]–maltol (dashed line) systems under identical conditions. pM = –log[M]; where [M] is the equilibrium concentration of the ligand-free, non-bound metal ions. *{c_M = 1 mM; M:L = 1:1; T = 25 ˚C; I = 0.20 M (KCl)}* Calculation for the Ru^{II}-containing system is based on data from [45].

Table 1

Crystal data and details of data collection for [Rh^{III}(Cp*)(allomaltolato)Cl] **1b**

Compound	**1b**
Empirical formula	$C_{16}H_{20}ClO_3Rh$
Formula weight / g/mol	398.68
Temperature / K	100(2)
Wavelength / Å	0.71073
Crystal size / mm	0.15 × 0.06 × 0.04
Crystal system	monoclinic
space group	$P2_1/c$
a / Å	8.0842(3)
b / Å	10.1198(4)
c / Å	19.2712(8)
α / °	90.00
β/ °	96.4400(13)
γ / °	90.00
Volume / $Å^3$	1566.64(11)
Z	4
Calculated density / mg/m^3	1.690

Absorption coefficient / mm^{-1}	1.267
F(000)	808
θ range for data collection	2.28–25.34°
Index ranges	$-9 \leq h \leq 9$
	$-12 \leq k \leq 12$
	$-23 \leq l \leq 23$
Reflections collected / unique	26776 / 2867
Data / restraints / parameters	2867 / 0 / 196
R(int)	0.0238
Goodness-of-fit on F^2 [a]	1.030
Final R indices [$I>2\sigma(I)$] [b]	
R_1	0.0331
wR_2	0.0946

[a] $GOF = \{\Sigma[w(F_o^2 - F_c^2)^2] / (n - p)\}^{1/2}$, where n is the number of reflections and p is the total number of parameters refined.

[b] $R_1 = \Sigma||F_o| - |F_c||/\Sigma|F_o|$. $wR_2 = \{\Sigma[w(F_o^2 - F_c^2)^2]/\Sigma[w(F_o^2)^2]\}^{1/2}$

Table 2

Overall stability constants ($\log\beta$) of the $[Rh^{III}(Cp^*)Z_3]$-hydroxido species at various ionic strengths (I) determined by pH-potentiometry {$T = 25$ °C}.[a]

	0.20 M KCl	**0.10 M KCl**	**0.20 M KNO_3**
log β (M_2H_{-2}) [b]	-11.12(1)	-10.48(2)	-8.53(7)
log β (M_2H_{-3}) [b]	-19.01(1)	-18.07(3)	-14.26(4)

[a] Standard deviations (SD) in parenthesis, values determined in aqueous solutions. [b] As H^+ is defined as a component, H_{-i} indicates the deprotonation of "i" coordinated H_2O molecules, or coordination of hydroxides.

Table 3

Proton dissociation constants (pK_a) of maltol and allomaltol and overall stability constants (log β) of their [Rh^{III}(Cp*)Z_3] complexes in chloride-containing and chloride-free solutions determined by pH-potentiometry {T = 25 °C; I = 0.20 M}.[a]

	maltol (1a)		**allomaltol (1b)**	
	0.20 M KCl	**0.20 M KNO_3**	**0.20 M KCl**	**0.20 M KNO_3**
pK_a (ligand)	8.44[b]	8.45(1)	7.97[c]	7.97(1)
log β [MLZ][d]	6.73(1)	8.45(1)	6.34(1)	8.01(1)
log β [MLH_{-1}][e]	-3.87(9)	-1.06(4)	–	-1.40(7)
pK [MLZ]	10.60	9.51	–	9.41
log K* [f]	-1.71	0.00	-1.63	0.04
log K (H_2O/Cl^-) [g]	1.17(1)		1.38(1)	

[a] Standard deviations (SD) in parenthesis, values determined in aqueous solutions. [b] Data taken from [42]. [c] Data taken from [44] [d] Z = H_2O or Cl^- for chloride-containing samples; Z = H_2O for chloride-free media. [e] As H^+ is defined as a component, H_{-1} indicates the deprotonation of a coordinated H_2O molecule, or coordination of OH^-. [f] log K* = log β [MLZ] − pK_a (HL). [g] $[Rh^{III}(Cp^*)(L)(H_2O)]^+ + Cl^- \rightleftharpoons [Rh^{III}(Cp^*)(L)(Cl)] + H_2O$ determined at various total chloride concentrations by UV-Vis spectrophotometry.

Table 4

In vitro cytotoxicity (IC_{50} values in μM) of the [Rh^{III}(Cp*)] complexes of maltol **1a** and allomaltol **1b** compared to their [Ru^{II}(η^6-*p*-cymene)] analogues [a]

	[Ru^{II}(η^6-*p*-cymene)] [b]		**[Rh^{III}(Cp*]**	
	maltol	***allomaltol***	**1a** ***(maltol)***	**1b** ***(allomaltol)***
CH1	81 ± 14	239 ± 22	120 ± 16	104 ± 20
SW480	159 ± 41	359 ± 119	178 ± 26	145 ± 5
A549	482 ± 20	518 ± 65	306 ± 34	280 ± 54

[a] 96 h exposure. [b] Data taken from [39].

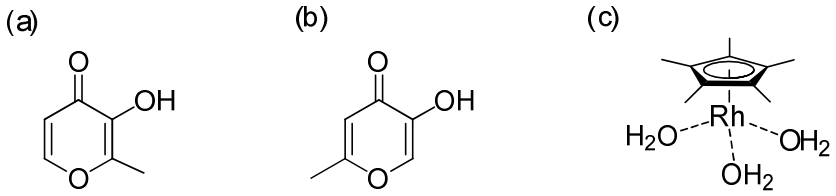

Chart 1

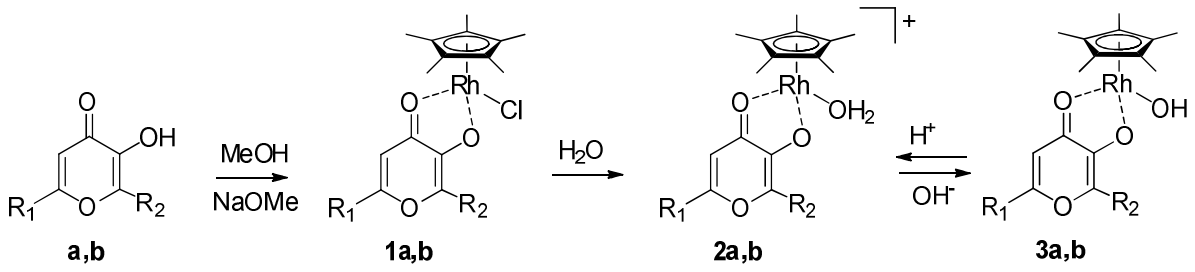

a: R_1 = H, R_2 = -CH_3 (Maltol)
b: R_1 = -CH_3, R_2 = H (Allomaltol)

Scheme 1

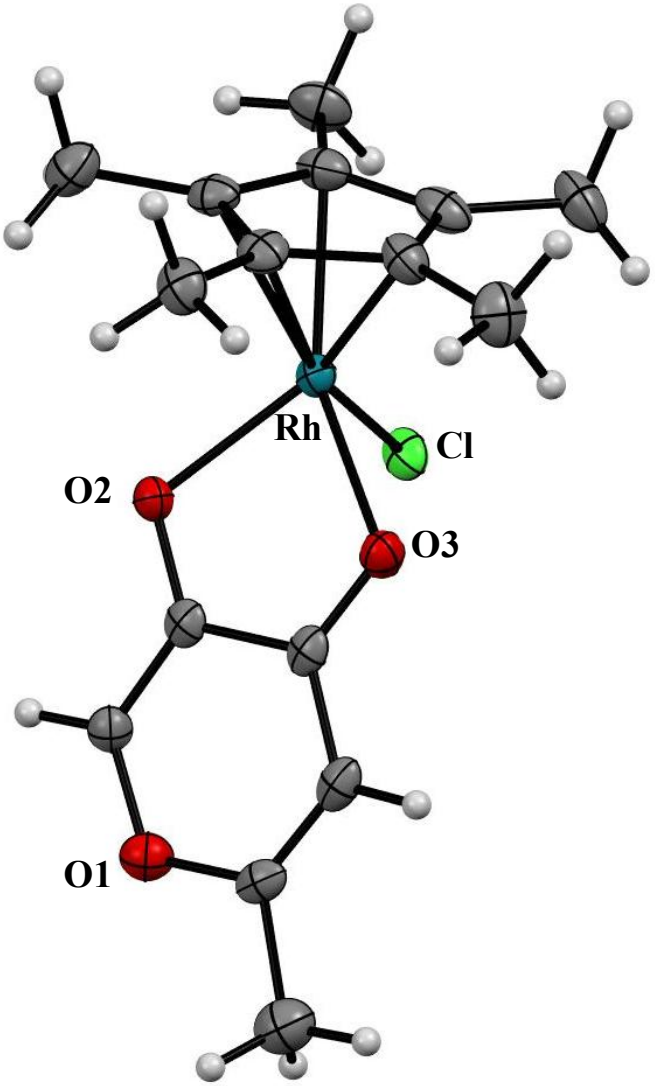

Fig. 1

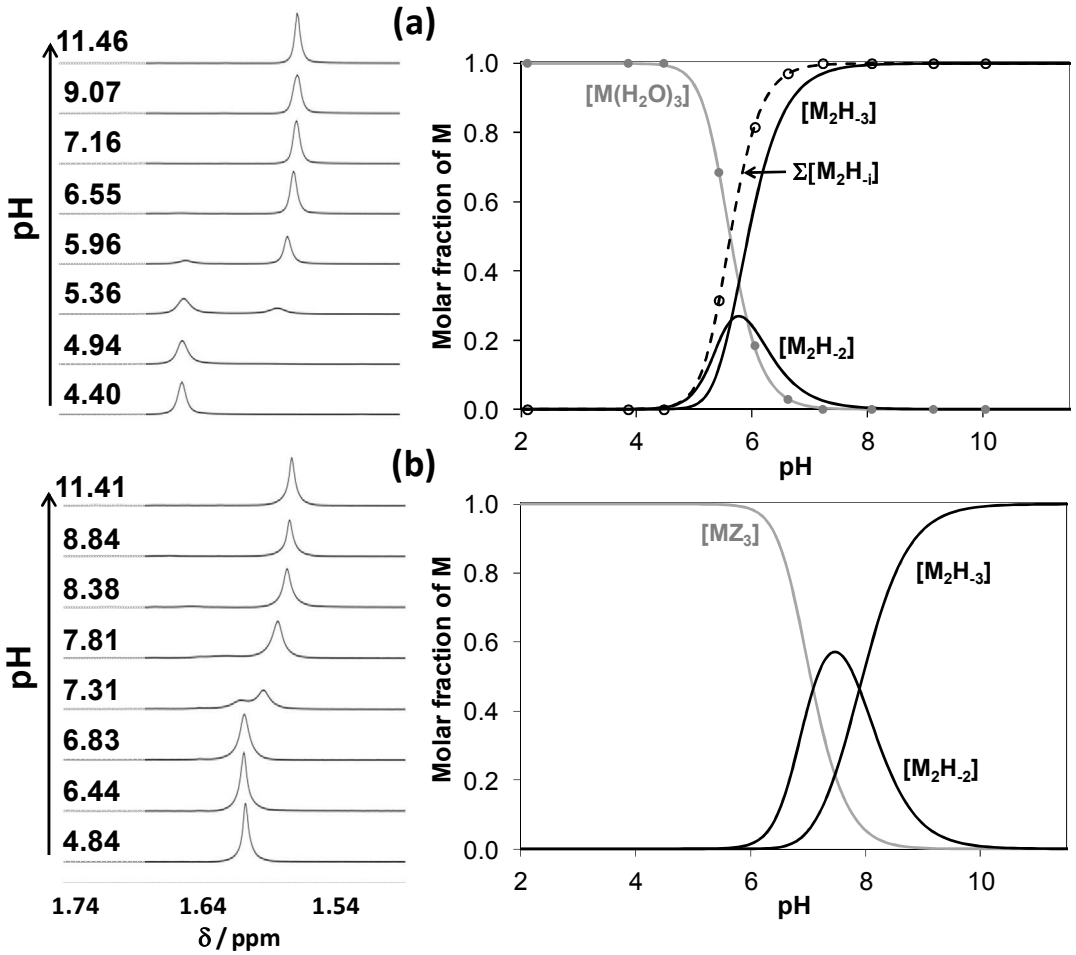
(a)
11.46
9.07
7.16
6.55
5.96
5.36
4.94
4.40
pH
Molar fraction of M
[M(H2O)3]
[M2H-3]
Σ[M2H-i]
[M2H-2]
pH
(b)
11.41
8.84
8.38
7.81
7.31
6.83
6.44
4.84
pH
[MZ3]
[M2H-3]
[M2H-2]
1.74
1.64
1.54
δ / ppm

Fig. 2

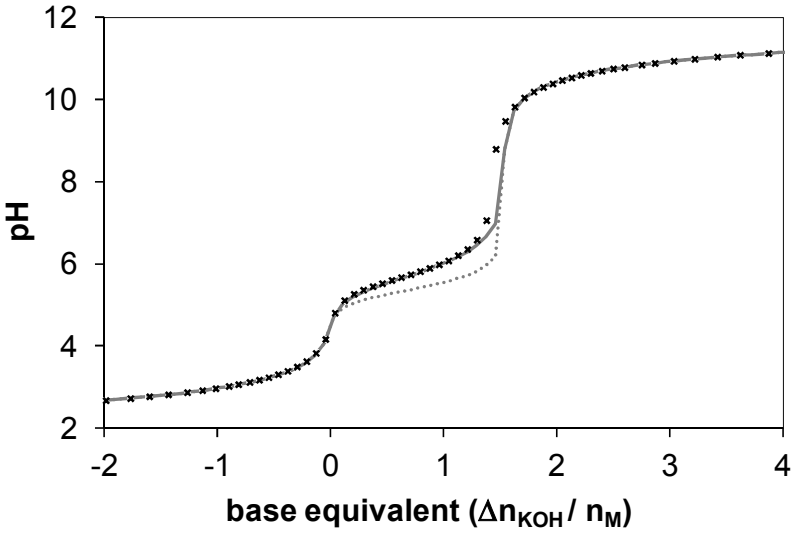
12
10
8
6
4
2
pH
-2
-1
0
1
2
3
4
base equivalent (Δn_KOH / n_M)

Fig. 3

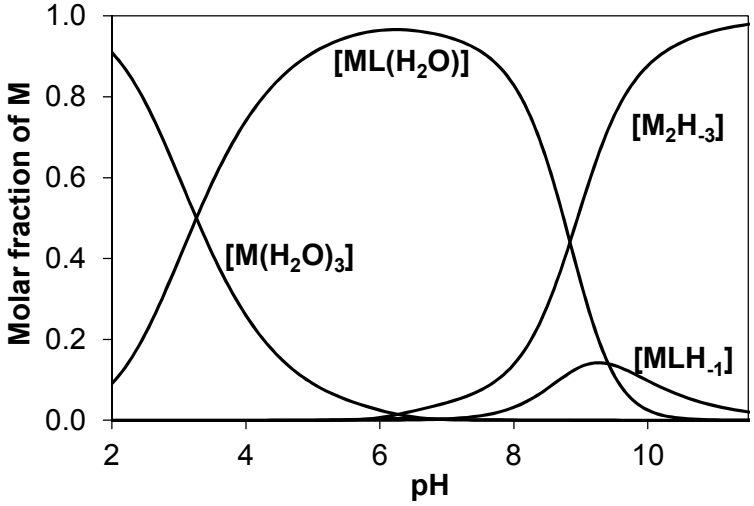
1.0
0.8
0.6
0.4
0.2
0.0
Molar fraction of M
[ML(H2O)]
[M2H-3]
[M(H2O)3]
[MLH-1]
2
4
6
8
10
pH

Fig. 4

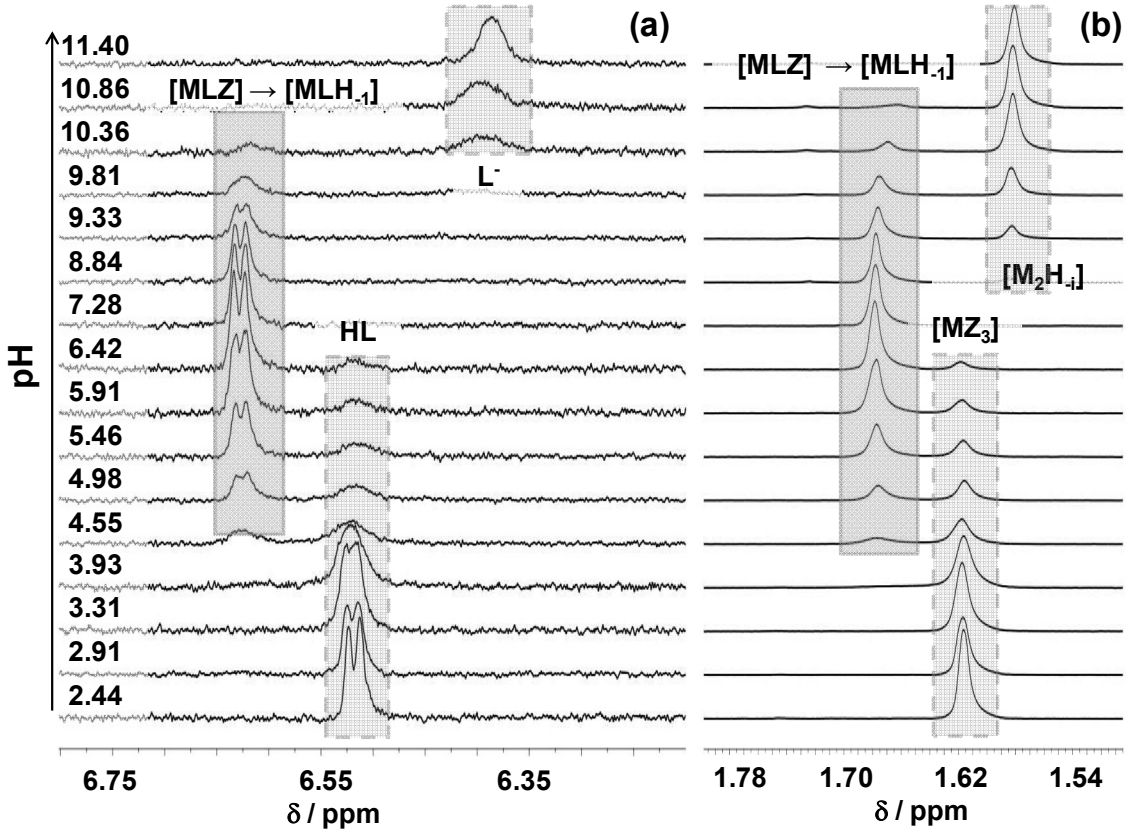
(a)
(b)
pH
11.40
10.86
10.36
9.81
9.33
8.84
7.28
6.42
5.91
5.46
4.98
4.55
3.93
3.31
2.91
2.44
[MLZ] → [MLH-1]
L-
HL
[MLZ] → [MLH-1]
[M2H-i]
[MZ3]
6.75
6.55
6.35
δ / ppm
1.78
1.70
1.62
1.54
δ / ppm

Fig. 5

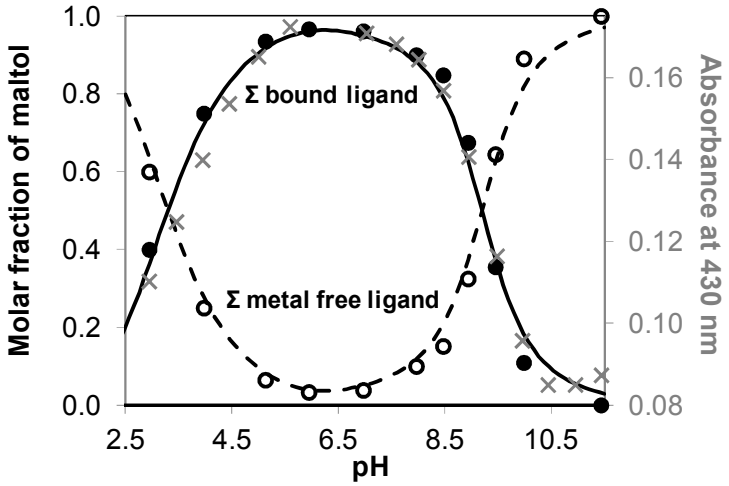
Molar fraction of maltol
Absorbance at 430 nm
pH
Σ bound ligand
Σ metal free ligand
1.0
0.8
0.6
0.4
0.2
0.0
0.16
0.14
0.12
0.10
0.08
2.5
4.5
6.5
8.5
10.5

Fig. 6

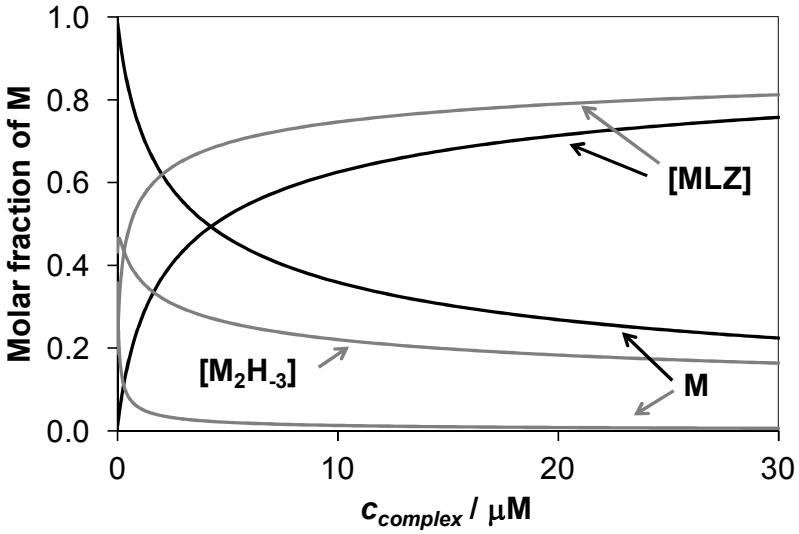
1.0
0.8
0.6
0.4
0.2
0.0
Molar fraction of M
[MLZ]
[M2H-3]
M
0
10
20
30
ccomplex / μM

Fig. 7

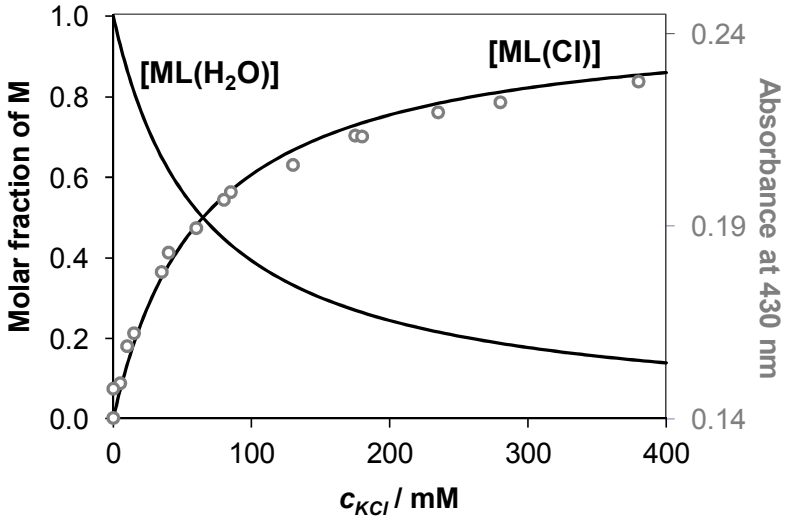
1.0
0.8
0.6
0.4
0.2
0.0
Molar fraction of M
[ML(H2O)]
[ML(Cl)]
0.24
0.19
0.14
Absorbance at 430 nm
0
100
200
300
400
cKCl / mM

Fig. 8

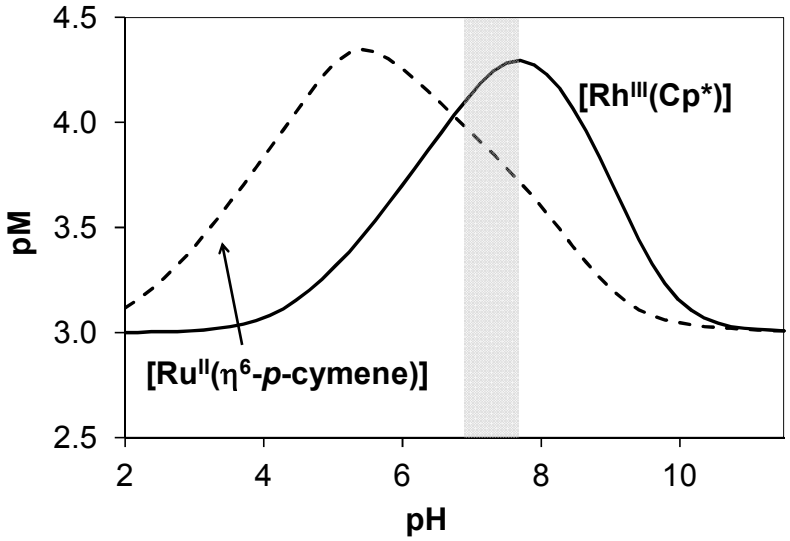

Fig. 9